 doi:10.20944/preprints202008.0184.v1

Article

Spatial Variability of Atmosphere Dust Fallout Flux in Urban-Industrial Environments

Maria de Lurdes Dinis [1,2,*], Maria Inês Gonçalves [2]

[1] CERENA/Porto - Centre for Natural Resources and the Environment; mldinis@fe.up.pt
[2] Faculty of Engineering, University of Porto; ega07076@fe.up.pt
* Correspondence: mldinis@fe.up.pt; Tel.: +351 22 041 3175 (M.L.D.)

Abstract: This work aimed to study the spatial variability of particulate matter deposition flux in urban-industrial environments. The main objective was to identify areas with higher deposition flux and associate the variability with climatological variables and with possible surrounding emitting sources. The method for collecting the deposited particles was based on the standard NF X 43-007. Sampling for particulate matter took place between April 2015 and February 2016, through seven sampling campaigns. Maps of the spatial dispersion for the particulate matter were obtained through statistics and geostatistics techniques. Elemental identification by scanning electron microscopy (SEM) was also used in two sampling campaigns. The results show that the sampling campaigns that took place during hot and dry periods, 2nd and 3rd, present higher deposition flux: 2.04 g/(m^2 x month) and 1.72 g/(m^2 x month), respectively. Lower deposition fluxes were registered in the 6th and 7th campaigns: 0.23 g/(m^2 x month) and 0.24 g/(m^2 x month), respectively. It was also observed a recurrent high deposition at specific sampling points which may be due to both the nearby road traffic and the presence of chimneys. SEM analysis allowed to associate repetitive element deposition, at the same sampling point, to the same emitting source.

Keywords: particulate matter; air quality; deposition flux; geostatistics; ordinary kriging; urban-industrial; elemental identification; electronic scanning microscopy

1. Introduction

Atmospheric particles, also known as particle pollution or PM, can be primary and secondary pollutants, forming a complex mixture of extremely small particles and liquid droplets. Particulate matter pollution comes from a variety of sources, which can be natural and anthropogenic. Natural sources include dust from soil and volcanoes, sprays of seawater, sand and dust from windstorms, pollens, spores, bacteria, plant fibres, etc. Particles from anthropogenic sources result from ash, tobacco smoke, soot and other particles produced mainly by the combustion of coal and fuel oil in industry and diesel motor vehicles. Particle pollution is made up of several components, including acids (such as nitrates and sulfates), organic chemicals, metals, and soil or dust particles [1].

The size of particles is one of the parameters that most influence the potential damage to human health. Those particles that are of 10 micrometers in diameter or smaller, generally pass through the throat and nose and enter the lungs. Once inhaled, these particles can affect the heart and lungs and cause serious health effects. Particles smaller than 2.5 μm are the most harmful to health, as they can penetrate deeply into the lungs during breathing and accumulate there. The deposited PM cannot be excreted immediately by the clearance mechanism of the human body and remains in place for a long time. Respiratory diseases are caused by PM deposition, especially in the alveolus [2].

Because of its complexity and the influence of particle size in determining the exposure and the resulting health effects, different terms are used to classify the particulate matter. Some are related to the sampling and/or analytical technique, e.g. "suspended particulate matter", "total suspended particulates", "black smoke". In contrast, others are related to the part of the affected respiratory track,

 doi:10.20944/preprints202008.0184.v1

e.g. "inhalable particles", which pass beyond the upper airways (nose and mouth), and "thoracic particles", which deposit within the lower respiratory tract [3].

According to the size, the particle pollution is generally referred to two main categories: i) those larger than 2.5 micrometers and smaller than 10 micrometers in diameter (particulate matter in which 50% of particles have an aerodynamic diameter of fewer than 10 μm – PM10), usually found near roadways and dusty industries - the "inhalable coarse particles" and ii) those found in smoke and haze, with 2.5 micrometers in diameter and smaller (PM2.5), such as directly emitted from sources such as forest fires, associated with gases emitted from power plants, industries and automobiles – the "fine particles". Another important characteristic is the chemical composition of PM. The presence of toxic compounds such as heavy metals, polyaromatic hydrocarbons and other carcinogenic substances can cause severe health problems, although compositions may change over time.

Concerning the damage to the environment, reduced visibility is the main problem, especially in urban areas. Particles deposition can cause damage to vegetation and watercourses, depending on the composition, concentration, toxicity or size, and it also has a negative impact on the external appearance of buildings and architectural monuments.

Source control is the only acceptable method for reducing particulate emissions. Regarding control technologies, these are mainly based on sedimentation, centrifugation, compaction, filtration processes and also through electrostatic precipitators. However, in an urban environment, particulate matter emerges from a wide range of natural and anthropogenic sources where it may be difficult to quantify the emissions and identify the sources. Also, particulate matter is produced by point and nonpoint sources which are affected by climatic factors, such as wind velocity, direction and frequency [4]. Therefore, there is a need to quantify the effect of ambient particulate matter loads in particular sites.

The present work focused on the study of the spatial variability of particulate matter flux deposition on the Polo II - Asprela Campus, of Porto University. Seven continuous sampling campaigns were carried out to collect particulate matter in strategic locations within the campus. The main objectives were to evaluate the deposition flux and determine potential contributing factors influencing the emissions and deposition.

2. Experiments

The adopted methodology followed four stages. The first stage concerns the definition of the sampling locations within the campus. The second stage involves the fieldwork developed to collect the particulate matter which was carried out in seven sampling campaigns, between April 2015 and February 2016. The third stage includes the laboratory work to remove the aerosols attached to the resin, filtration and weighing the collected material to calculate the deposition flux (mass/time x area). At the final stage, the particulate matter was analyzed by Scanning Electron Microscopy (SEM).

A statistical analysis was applied to the obtained results for the deposition flux, combined with the local meteorological data registered during each one of the sampling periods. The study involved classical statistics and geostatistics techniques to assess the directional behaviour of the deposition flux as well as the behaviour and interference of the variables likely to influence the deposition of particulate matter.

2.1. Study Area

The university campus of Asprela is located in the parish of Paranhos, with an area of about 145 hectares (Figure 1). Currently, the Asprela campus is dominated by 21 educational, health and research institutions, mostly composed of the faculties and research centers of Porto University. The Polytechnic Institute of Porto has also installed two of its faculties in this area, and the Portuguese Catholic University has on-campus its second University Pole, linked to science and health.

In addition to university facilities, there are other services such as hospital facilities: Hospital S. João and Oncological Porto Institute (IPO). Both are responsible for much of the daily traffic in the area. There is high daily affluence to the campus through the accesses from the N12 ring road and

Preprints (www.preprints.org) | NOT PEER-REVIEWED | Posted: 7 August 2020 doi:10.20944/preprints202008.0184.v1

the A3 and A20 motorways. Regarding access through public transport, it can be easily done by subway and bus services.

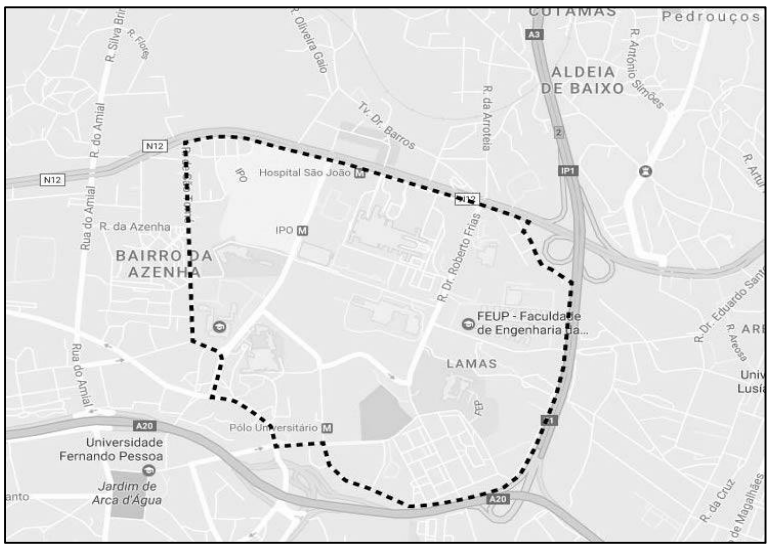

Figure 1. University campus of Asprela (Google Earth, 2017).

2.2. Sampling Site

The assessment of the dispersion and deposition of particulate matter focused essentially on potentially critical areas within the Asprela's campus: campus parking lots, socializing and student's living areas (high turnout area), outside eating facilities and athletic fields (low traffic) and low turnout area students representing the "background" site (used as the blank or control sampling points). Therefore, 35 sampling points, considered as critical within the campus area, were defined to place the particulate matter collectors (Figure 2).

Figure 2. Sampling area within the Asprela's University Campus (Google Earth, 2017).

The locations of the sampling points were adapted in many cases to the field conditions (access to the locations and the existence of conditions to place the collectors), as well as the risk of being removed (some sampling points were located in inhabited areas). The identification of each sampling point and the possible emission source is presented in Table 1.

 doi:10.20944/preprints202008.0184.v1

112 **Table 1.** Identification of the sampling points (SP) and the influence of possible emission sources.

SP Nº		Sampling location	Possible emission source
1	**FEUP**	Buildings F/G	Smoking Area, Road Traffic
2		Library	Smoking Area, Road Traffic
3		Parking Lot P3	Road Traffic
4		Canteen	Chimneys, Road Traffic
5		Students Association FEUP	Smoking Area
6		Parking Lot P1	Road Traffic
7		Cafeteria	Chimneys, Road Traffic
8		INESC	Road Traffic
9		Bicycle Path	Green Area, Road Traffic
10	**FEP**	Parking Lot Staff	Road Traffic
11		Parking Lot Students	Road Traffic
12		Students Association FEP	Green Area
13	**CREMATORIUM**	Crematorium	Chimneys, Road Traffic
14	**FADEUP**	Grass park	Green Area
15		Entrance	Smoking Area
16		Parking Lot	Road Traffic
17		Football Field	Green Area
18	**IPATIMUP**	Entrance	Road Traffic
19		Parking Lot	Road Traffic, Chimneys
20		Buildings	Green Area
21	**ESE**	Tennis Field	Green Area, Road Traffic
22		Entrance	Green Area, Smoking Area
23		Parking Lot	Road Traffic
24		Buildings	Green Area, Smoking Area
25		Grass Park	Green Area, Chimneys
26	**H. SÃO JOÃO**	Entrance	Smoking Area, Road Traffic
27		Paediatrician Service	Construction Works, Chimneys
28		Gynaecologic/Obstetric Service	Road Traffic
29		Students Association FMUP	Construction works, Road Traffic
30	**ESEP**	Entrance	Green Area, Road Traffic, Subway Line
31		Parking Lot	Road Traffic
32	**ISEP**	Entrance	Green Area, Road Traffic
33		Buildings	Smoking Area, Road Traffic
34		Parking Lot	Road Traffic
35	**FDMUP**	FMDUP	Road Traffic

113

114 The sampling duration, as well as the starting and finishing dates, are presented in Table 2.

115

116

117

118

Preprints (www.preprints.org) | NOT PEER-REVIEWED | Posted: 7 August 2020 doi:10.20944/preprints202008.0184.v1

Table 2. Sampling campaigns duration.

Sampling Campaign Nº	Initial date	End date	Nº days
1	13 April	14 May	32
2	11 May	17 June	38
3	15 June	22 July	38
4	20 July	12 October	85
5	07 October	20 November	45
6	16 November	19 January	65
7	15 January	19 February	35

2.3. Particulate matter collection methodology

The collection of particulate matter was carried out by a passive collection system following the French standard NFX43-007 (1973). This methodology consists of a 50 cm^2 stainless steel slice horizontally fixed at a defined height above the ground with a silicone cover (Polydimethylsiloxane) to trap dust fallout. The same sampling procedure was carried out at sampling points selected as a control, theoretically away from the possible influence of anthropogenic sources. About 35 slices were placed in the study area at approximately 2.5 meters above the ground. This height above the ground was adopted to assure that the collectors were recovered without being damaged.

Seven sampling campaigns (SC1-SC7) were carried out in the study area between April 2015 and February 2016. A month was chosen for the collection of the particulate matter and the determination of the deposition flux, taking into consideration the logistic factors of placing and removing the collectors. For the SC4 and SC6, the exposure time was longer than one month due to the closing of some Faculties for vacations. Sampling point Nº 35 was cancelled, after SC3, because the collector disappeared twice.

After the exposure period, the aerosols attached to the resin were removed at the laboratory. The collectors were rinsed with an organic solution (dichloromethane) and filtered in a glass filtration system (Buchner funnel) over a 0.22 μm Polyvinylidene Difluoride (PVDF) membrane filters with 47 mm diameter. Filters were dried and weighted to obtain the particle deposition flux expressed in weight per unit area per unit time (g m^{-2} $month^{-1}$).

2.4. Scanning Electron Microscopy Analysis – SEM

The SEM studies were carried out at the Scanning Electron Microscopy and Microanalysis Laboratory, Microstructure and Microanalysis Unit - IMICROS at the Materials Center of the University of Porto (CEMUP). The equipment used was a high-resolution Environmental Scanning Electron Microscope (Schottky), with X-Ray Microanalysis and Analysis of Diffraction Patterns of Retro-fused Electrons: FEG-ESEM / EDS / EBSD.

The methodology adopted for SEM samples preparation consisted of selecting the region of each filter, with the most substantial amount of particles. Sections of 1.5 mm by 1.5 mm were cut with scissors from this region and mounted with double-sided tape on a copper plate.

The SEM analysis was carried out in two sessions for the particulate matter collected during SC2 and SC3. For the first session, 33 samples from SC2 were analyzed and for the second session, seven samples from SC3 were selected. These two sampling campaigns were selected based on the amount of particulate matter collected.

2.5. Meteorological data

Meteorological data was continuously collected from three fixed stations located a few kilometers from the campus: 06F/03UG (~7 km); LPPR 1400/1408 (~9 km); and 06E/03UG (~19 km). These stations are the closest to the sampling site with free available data. Daily average, maximum and minimum values were automatically extracted for temperature, rainfall, wind velocity and direction. The WRPLOT View™ software was used to generate the wind rose with the collected meteorological data.

Preprints (www.preprints.org) | NOT PEER-REVIEWED | Posted: 7 August 2020 doi:10.20944/preprints202008.0184.v1

159 *2.6. Data analysis tools*

160 Maps on the spatial distribution of the dust fallout flux were developed for the study area,
161 through the use of geostatistical interpolation techniques. The ordinary kriging was applied to create
162 the prediction map of the spatial dispersion performed with Golden Software Surfer 8.0.

163 **3. Results**

164 *3.1. Climatological data*

165 Data for wind direction, precipitation and average wind speed were extracted from the
166 meteorological stations and is presented in Table 3, Figure 3 and Figure 4. For wind characteristics,
167 rose winds per each sampling campaign were also generated (Figure 5 - Figure 11).

168 **Table 3.** Data of the meteorological characteristics verified during the sampling campaigns.

SCNº	Wind Direction (°)				Wind Velocity (m/s)				Temperature (°C)				Rainfall (mm)			
	μ	± σ	Min.	Max.	μ	± σ	Min.	Max.	μ	± σ	Min.	Max.	μ	± σ	Min.	Max.
1	186	31	129	259	0.4	0.4	0.0	1.7	15	2	12	21	0.3	1.8	0.0	10.1
2	216	26	150	285	0.1	0.2	0.0	0.7	18	3	14	25	1.0	5.4	0.0	33.6
3	206	19	168	240	0.1	0.1	0.1	0.4	19	2	17	27	0.0	0.0	0.0	0.0
4	193	34	119	244	0.3	0.7	0.0	3.2	17	1	14	20	4.4	15.7	0.0	96.3
5	179	39	109	250	1.2	1.2	0.0	4.0	16	2	13	20	3.7	9.3	0.0	49.2
6	199	43	69	295	2.7	1.1	0.9	5.1	13	2	8	18	9.0	11.0	0.0	43.2
7	181	67	69	303	2.0	1.0	0.6	4.5	11	3	6	17	4.8	7.3	0.0	23.4

169

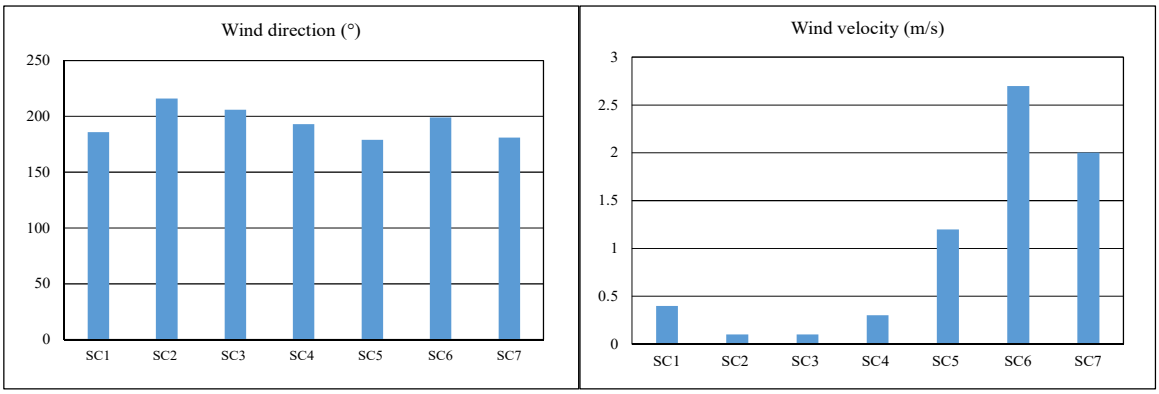

170

171 **Figure 3.** Wind direction and wind velocity of each sampling campaign.

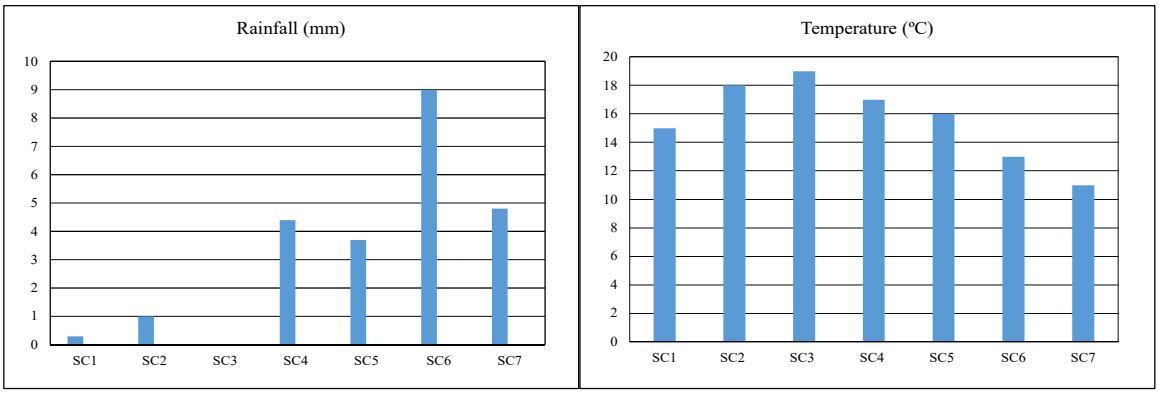

172

173 **Figure 4.** Rainfall and temperature of each sampling campaign.

Preprints (www.preprints.org) | NOT PEER-REVIEWED | Posted: 7 August 2020 doi:10.20944/preprints202008.0184.v1

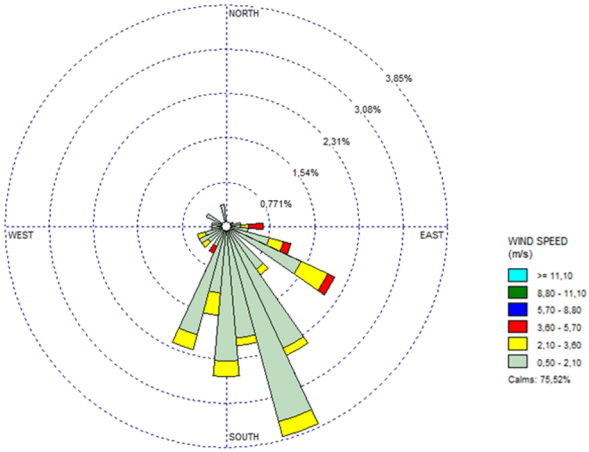

174

175 **Figure 5.** Rose winds (direction and average wind speed) for SC1 period.

176 In April 2015 (SC1), the average temperature (15.08 °C) was above the normal value by about 2
177 °C, being the 3rd highest value in the last 18 years. In May, the average value of the average
178 temperature was 18.67 °C, an anomaly of about more 3 °C, being the second-highest value since 1931.
179 According to the climatological bulletins for Portugal, April and May 2015 were considered very
180 hot and dry months. Rainfall was on average of low intensity which promoted the deposition of
181 particulate matter and, therefore, had a minor effect on the washout of the deposited particulate
182 matter. Rainfall was, on average, much lower than typical values for this time of the year, showing
183 the drought situation occurring throughout the national territory since February. Regarding wind
184 direction, it was predominantly from NW-N to SE-S and the wind speed recorded during this period
185 is characterized by its low intensity, with an average of 0.1 m/s.
186 June 2015 (SC2) was the warmest month in the last 10 years. The average temperature during
187 this month was 21.85 °C, and in May, it was 18.67 ºC, so this sampling period can also be characterized
188 as hot. In average, the precipitation was 1.0 mm and, on most days, there was no precipitation at all
189 and, therefore, this period can be considered as dry. Nevertheless, the maximum value for total daily
190 precipitation was 33.6 mm registered on June 14. This day was probably unfavorable regarding the
191 deposition of particulate matter, due to the washout. However, this effect will appear diluted in the
192 monthly deposition flux. In this campaign, the wind direction was predominantly to south, in
193 particular towards SW. The wind speed during this period was characterized, again, by its low
194 intensity, with an average of 0.1 m/s where for 17 days in a row the wind speed was approximately
195 0.0 m/s, so this campaign took place in a period characterized by "very light wind".
196

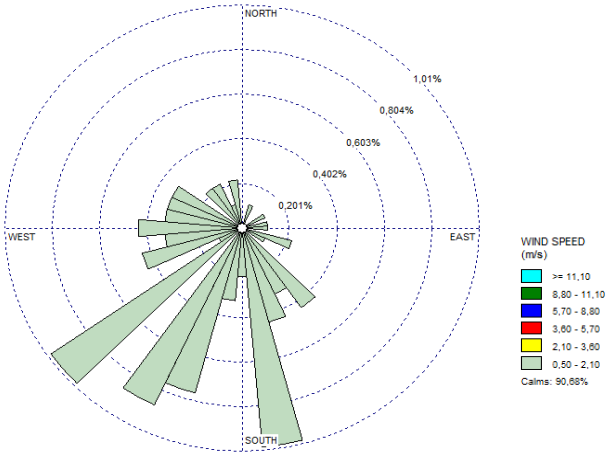

197

198 **Figure 6.** Rose winds (direction and average wind speed) for SC2 period.

Preprints (www.preprints.org) | NOT PEER-REVIEWED | Posted: 7 August 2020 doi:10.20944/preprints202008.0184.v1

The SC3 was also characterized as hot and dry weather. No rainfall events occurred during this period (from 15 June to 22 July).

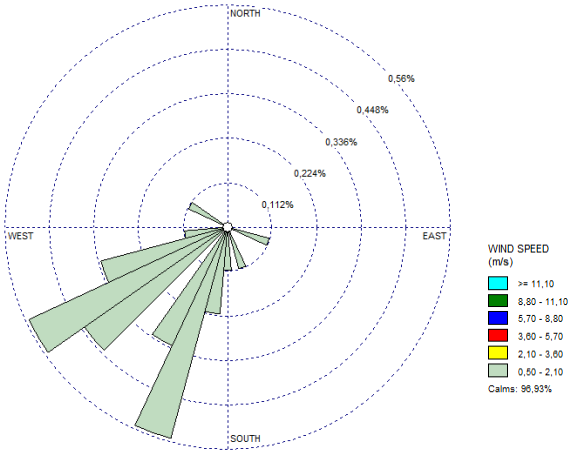

Figure 7. Rose winds (direction and average wind speed) for SC3 period.

Wind direction was predominantly from NE to SW. This period was characterized by calm winds with an average of 0.1 m/s. During SC3, the wind speed was approximately 0.0 m/s for 20 days in a row.

The SC4 was the longest one with a duration of 85 days. This sampling period was characterized as cold and dry with a few rainfall events. Wind direction was predominantly to SW. Wind velocity was also more expressive in this sampling campaign.

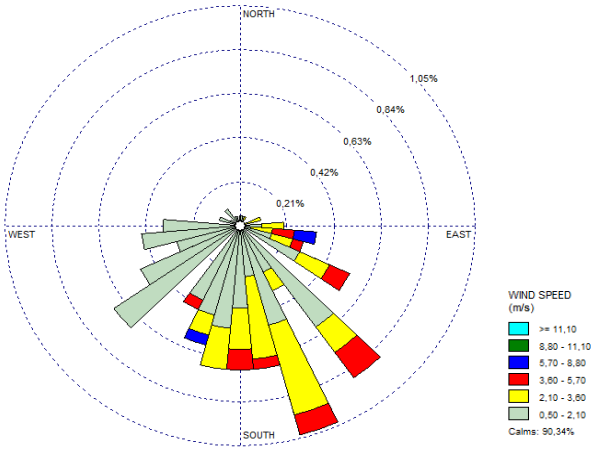

Figure 8. Rose winds (direction and average wind speed) for SC4 period.

For SC5, the weather was also considered as warm, although this sampling campaign went throughout the autumn season. Most of the rainfall events occurred during October, and in particular at the end this month. Wind direction was predominate to SW although in some situations the direction was also to SE. Wind velocity starting to show higher maximum values since SC4, for this period.

Preprints (www.preprints.org) | NOT PEER-REVIEWED | Posted: 7 August 2020 doi:10.20944/preprints202008.0184.v1

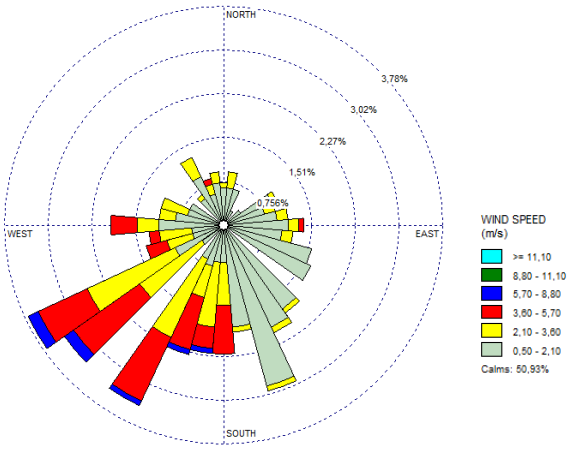

Figure 9. Rose winds (direction and average wind speed) for SC5 period.

In what concerns the period of SC6, it was also considered a hot or warm one with higher rainfall events, in particular, during January, where there were only four days without rainfall. Maximum rainfall value (43.2 mm) was registered during January. Concerning the wind direction, during this period it was predominantly to south. Higher values for the wind velocity were registered during this sampling campaign (3.50-5.70 m/s).

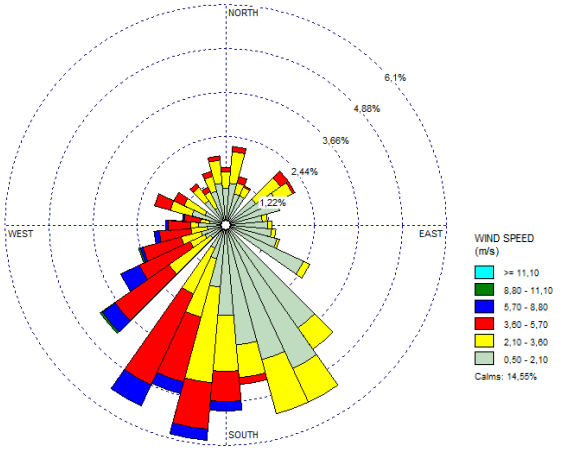

Figure 10. Rose winds (direction and average wind speed) for SC6 period.

The last sampling campaign, SC7, was carried out also through a rainy period, with 4.8 mm of precipitation, and wherein only 12 out of 35 days there was no precipitation. For the wind direction, there was a variation mostly in all directions.

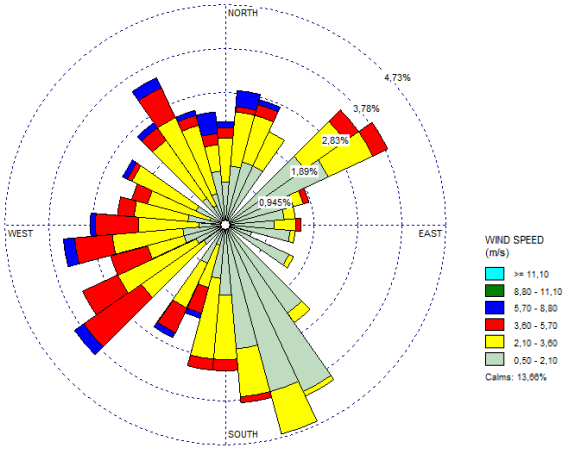

Figure 11. Rose winds (direction and average wind speed) for SC7 period.

Preprints (www.preprints.org) | NOT PEER-REVIEWED | Posted: 7 August 2020 doi:10.20944/preprints202008.0184.v1

3.2. Particulate matter deposition flux

The results of the deposition flux for each sampling campaign are presented in Figure 12.

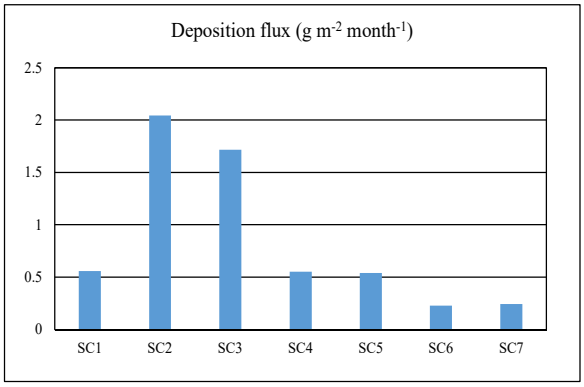

Figure 12. Deposition flux of each sampling campaign (g m^{-2} $month^{-1}$).

The statistical characteristics are shown in **Error! Not a valid bookmark self-reference.**.

Table 4. Statistical characteristics of the calculated deposition flux.

Deposition flux (g m^{-2} $month^{-1}$)	Mean	± σ	Median	Min.	Max.
SC1	0.5585	0.6271	0.2930	0.0018	3.1390
SC2	2.0449	0.9913	1.9006	0.7355	4.3518
SC3	1.7165	0.7650	1.7115	0.1646	3.9866
SC4	0.5531	0.8507	0.3006	0.0145	4.6712
SC5	0.5399	0.6068	0.3792	0.0897	2.6613
SC6	0.2298	0.2452	0.1596	0.0199	1.4149
SC7	0.2434	0.3096	0.1865	0.0169	1.8685

The deposition flux was higher during SC2 and SC3 and much lower during SC6 and SC7, which can be explained by the variation of the meteorological conditions. Both sampling campaigns, SC2 and SC3, were characterized by hot and dry months, with higher temperature values than usually for the same period in previous years. Rainfall was scarce according to the meteorological drought registered for seven months with only minor rainfall events only in SC2.

In SC6 and SC7 several events of heavy rainfall occurred although the SC6 experienced higher temperatures than the normal for this season. Both campaigns were characterized by intense and sometimes continuous precipitation periods.

3.3. Spatial dispersion for particulate matter deposition flux

Data from the particulate matter collected in SC1 were discarded from the study as the filters were damaged during the laboratory procedure.

The spatial distribution of the dust deposition fluxes for SC2 and SC3 are presented in **Figure 13**.

Preprints (www.preprints.org) | NOT PEER-REVIEWED | Posted: 7 August 2020 doi:10.20944/preprints202008.0184.v1

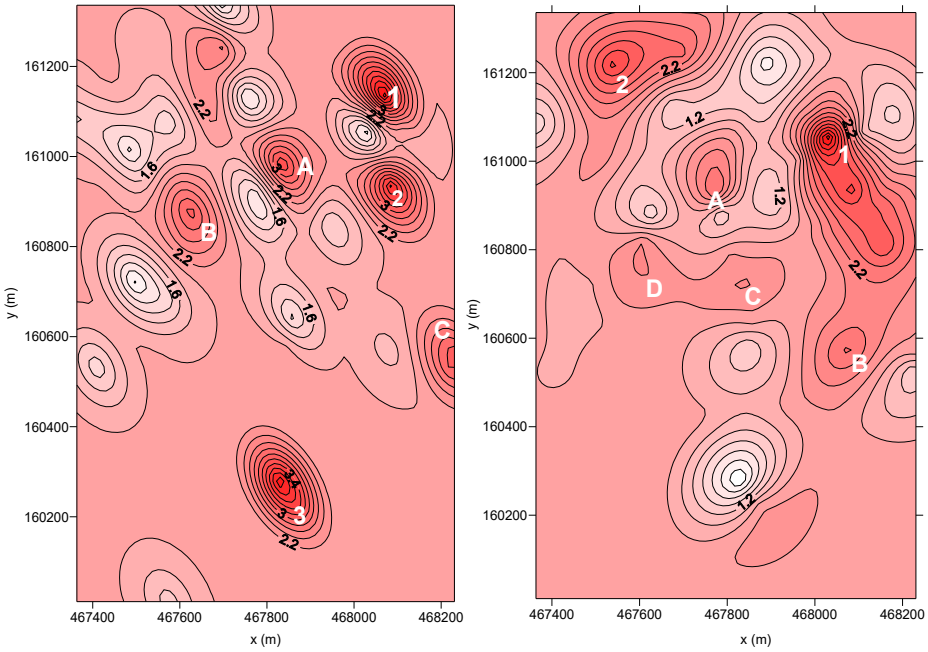

Figure 13. Spatial distribution of the dust flux deposition: a) SC2 and b) SC3.

From the dispersion of the deposition flux of SC2, it is possible to observe that there are three points with preferential deposition and three additional preferential deposition areas (A, B, C):

- Point Nº 1 - corresponds to SP24, placed in a green area but also near a smoking spot.
- Point Nº 2 - located in the Hospital São João and refers to SP28. This area is highly exposed to road traffic.
- Point Nº 3 - has the contribution of both SP33, placed in smoking and road traffic zones, and SP34, set in a zone also influenced by the road traffic.
- A - Corresponds to SP7, the cafeteria of the Faculty of Engineering. Here, the deposition flux is influenced by the car traffic of the parking lot - P1 (SP6) and the chimneys of the cafeteria.
- B - Includes the parking lot of the Faculty of Economics (SP10) and the Crematorium of Paranhos (SP13). Both are located facing Dr Roberto Frias Street, a road with high traffic, which may be the justification for the obtained values. Regarding the Crematorium, the high deposition of particles can be explained by the presence of the incineration chimneys.
- C - Corresponds to the sampling points of the Nursery School (ESEP - SP 30 and SP31). The high amount of particulate matter collected in this area can be justified by the road traffic and the presence of the subway line as well. During this sampling campaign, the wind direction was predominantly towards SE, where ESEP is located.

Table 5. Possible sources of high deposition flux – SC2.

Designation	SP	Source/cause of the deposition flux
1	24	Smoking area
2	28	Road traffic
3	32	Road traffic
	33	Smoking area
A	7	Road traffic
		Smoking area
B	10	Road traffic
	13	Incineration chimneys
C	30	Road traffic
	31	Subway line

Preprints (www.preprints.org) | NOT PEER-REVIEWED | Posted: 7 August 2020 doi:10.20944/preprints202008.0184.v1

From the dispersion of the deposition flux from SC3, it is possible to observe that are two points with preferential deposition and four wider deposition areas (Zone A, B, C and D):

- Point Nº 1 - includes SP23 (parking lot ESE) and SP28 (Hospital São João). This zone is highly exposed to road traffic.
- Point Nº 2 - corresponds to the SP7 (FEUP's cafeteria) and the deposition flux at this spot is influenced by both the car traffic of the parking lot P1 (SP 6) and the chimneys of the cafeteria.
- A - Corresponds to SP6 (parking lot P1).
- B - is located in the Student Association of the Faculty of Engineering, SP5, which corresponds to a smoking spot.
- C - Corresponds to the Crematorium of Paranhos (SP13), influenced by the incineration chimneys and the road traffic as well.
- D - Corresponds to the parking lot of the Faculty of Sports (SP16.

Table 6. Possible sources of high deposition flux – SC3.

Designation	SP	Source/cause of the deposition flux
1	23 28	Road traffic
2	7	Road traffic Chimneys
A	6	Road traffic
B	5	Smoking area
C	13	Road traffic Incineration chimney
D	16	Road traffic

The spatial distribution of the dust deposition fluxes for SC4 and SC5 are represented in Figure 14.

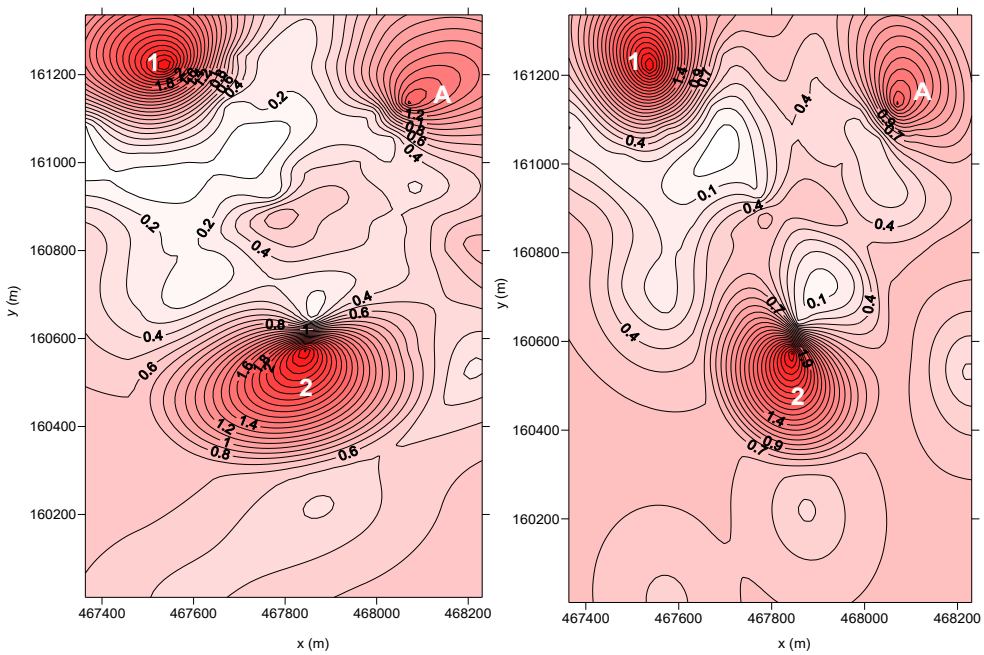

Figure 14. Spatial distribution of the dust flux deposition: a) SC4 and b) SC5.

From the dispersion of the deposition flux of SC4 it is possible to observe that are two points with preferential deposition and one wider deposition area (Zone A):

- Point Nº 1 - corresponds to SP7 (FEUP's cafeteria).

Preprints (www.preprints.org) | NOT PEER-REVIEWED | Posted: 7 August 2020 doi:10.20944/preprints202008.0184.v1

- Point Nº 2 - corresponds to the SP18 (IPATIMUP's building) located near a high traffic zone (parking lot and Dr Roberto Frias Street). During this sampling period, wind direction was towards south coincident with the location of the collector.
- A - Includes the SP25 surrounded by the canteen chimneys of the ESE.

In SC5 two points were identified as high deposition flux spots and one wider area (Zone A):

- Point Nº 1 - corresponds to SP7 (FEUP's cafeteria).
- Point Nº 2 - corresponds to SP18 (IPATIMUP's building).
- A - Includes the SP25 surrounded by the canteen chimneys of the ESE.

Table 7. Possible sources of high deposition flux – SC4.

Designation	Sampling location Nº	Source/cause of the deposition flux
1	7	Road traffic, chimneys
2	18	Road traffic
A	25	Chimneys

The spatial distribution of the dust deposition fluxes for SC6 and SC7 are represented in Figure 15.

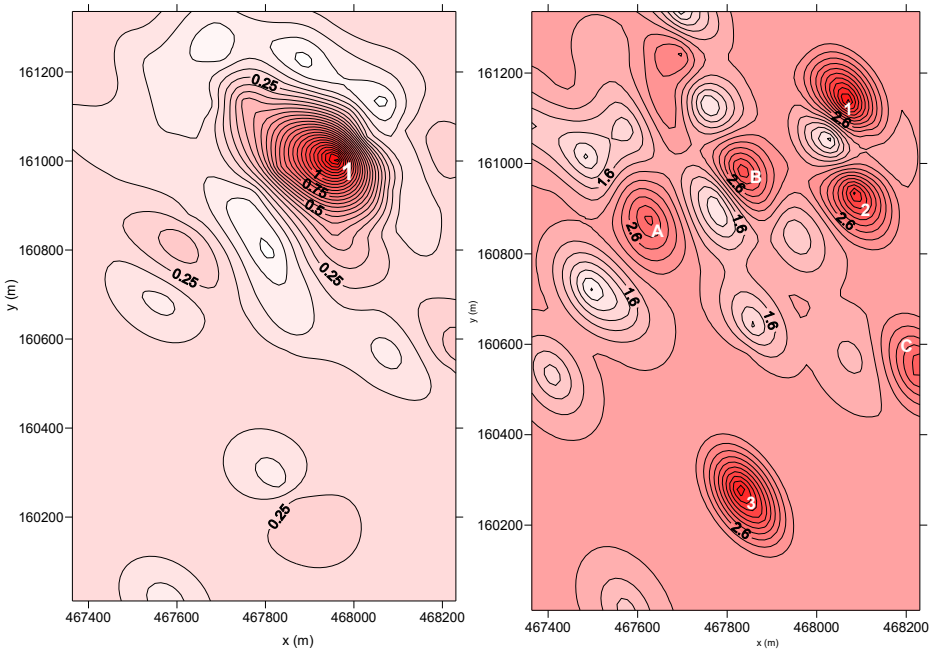

Figure 15. Spatial distribution of the dust flux deposition: a) SC6 and b) SC7.

For the dispersion of the deposition flux collected in SC6 it is possible to observe only one point with preferential deposition. For the dispersion from SC7 three preferential deposition points and three wider deposition areas (zone A, B and C):

- Point Nº 1 - includes SP23 (parking lot) and SP28 (Hospital São João). This zone is highly exposed to road traffic. During this sampling campaign, there were several raining events which may have promoted the washing of the dust fallout, decreasing the total collected flux.

From the last sampling campaign (SC7), it is possible to observe that there are three points with preferential deposition and three preferential deposition areas (A, B, C):

Preprints (www.preprints.org) | NOT PEER-REVIEWED | Posted: 7 August 2020 doi:10.20944/preprints202008.0184.v1

Table 8. Possible sources of high deposition flux – SC7.

Designation	SP	Source/cause of the deposition flux
1	25	Smoking area
2	28	Road traffic
3	33	Road traffic
	34	Smoking area
A	10	Road traffic
	13	Incineration chimneys
B	7	Road traffic, chimneys
C	30	Road traffic
	31	Subway line

3.4. Particulate matter analysis by SEM

Based on the elemental composition and morphology, the collected particles may be associated with different groups according to their origin: geogenic, anthropogenic, and biogenic. Geogenic particles consist of natural particles with crustal origin. They are comprised of quartz, aluminosilicates, calcium-rich particles, chloride-based particles, and iron/titanium oxides. The anthropogenic group include carbonaceous and industrial particles, and their origin is mostly from local emissions. Biogenic aerosols included particles of biological nature, dead or alive, such as spores, pollen, and plant debris and animal matter. Usually, biological particles consist of minor amounts of elements like Na, Mg, K, Ca and Cl, and major amounts of C and O.

Aluminosilicates are minerals containing aluminium oxide (Al_2O_3) and silica (SiO_2) and are present in ~72% of the total chemical compounds in Earth's crust [5, 6]. The soil-derived aluminosilicates particles are generally composed of Si and Al oxides with varying amounts of Na, K, Mg, Ca, Fe, and Ti. Aluminosilicates particles may present different shapes and sizes: triangular-shaped (biotite), trapezium-shaped (K-feldspar), soap-like (Na-feldspar), and tablet-like (Calcium magnesium aluminosilicate). They are used as a raw material in the manufacture of cement, glass and ceramics (Schumann, 2001). Aluminosilicates particles were identified in SP7, SP8, SP9, SP14, SP19, SP22, SP23 and SP35 (Figure 16-a and Figure 16-b).

Biotite is a common mineral in the silicate class, phyllosilicate subclass, micas group and ferromagnesian subgroup, which contains potassium, magnesium, iron and aluminium in its composition: $K(Mg, Fe)_3(OH, F)_2(Al, Fe)(Si_3O_{10})$. Biotite has a small number of commercial uses, it is used in the manufacture of paints, as an additive in drilling muds, in the production of rubber products and as a non-stick surface coating on asphalt shingles and roofs. Biotite particles were identified in SP8 (Figure 16-c).

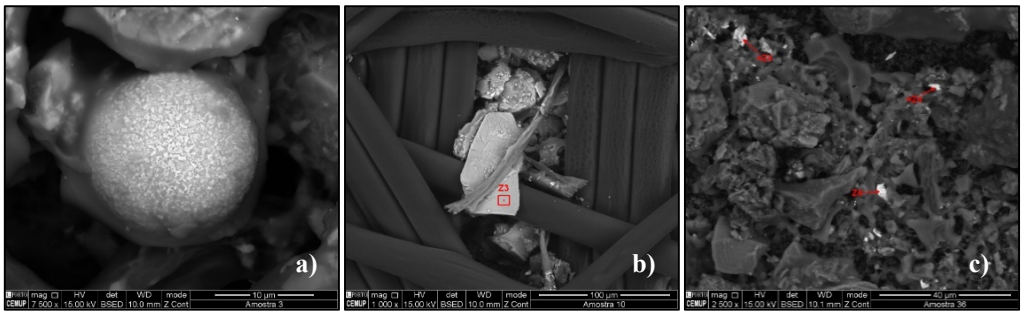

Figure 16. Scanning Electron Microscopy images of aluminosilicates particles-a), b) and biotite particle-c).

Silicon (Si) is the second most abundant element on the Earth's crust, making up more than 28% of its mass. It appears in clay, feldspar, granite, quartz and sand, usually in the form of silicon dioxide (SiO_2) and silicates (compounds containing silicon, oxygen and metals). Silicon is the main component of glass, cement, ceramics and silicones. Pure Si particles are of natural origin as well as artificial origin. In the Earth's crust, Si is a component of sandstone and granite. Most of the

Preprints (www.preprints.org) | NOT PEER-REVIEWED | Posted: 7 August 2020 doi:10.20944/preprints202008.0184.v1

construction materials are minerals that contain silicon in their composition. Silicon particles were identified at SP17, SP25 and SP37 (Figure 17-a and Figure 17-b).

Quartz (SiO_2) is formed by 46.7% of silicon and 53.3% of oxygen. It is an almost pure chemical compound and has constant properties. The primary origin of quartz in the atmosphere is soil, but it is also found in building materials such as cement, glass, ceramic, bricks, and clays. Quartz particles were identified in SP32 (Figure 17-c).

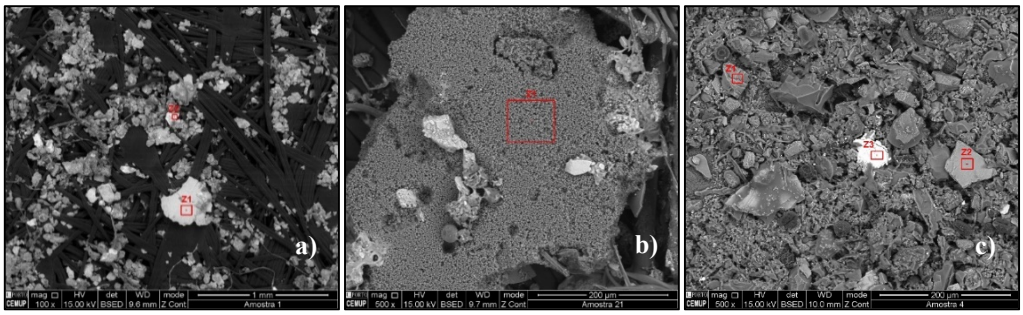

Figure 17. Scanning Electron Microscopy images of silicon particles-a), b) and-c) quartz particles.

Zircon ($ZrSiO_4$) is a mineral belonging to the group of nesosilicates (zirconium silicate). Heavy mineral suites, represented by zircon, provide valuable evidence about the origin of sediment and interpretation of their provenance [7]. Zircon reflects the granitic igneous rock origin. Zircon particles were identified in SP2, SP4, SP5, SP8, SP23, SP24, SP26, SP29 and SP30 (Figure 18).

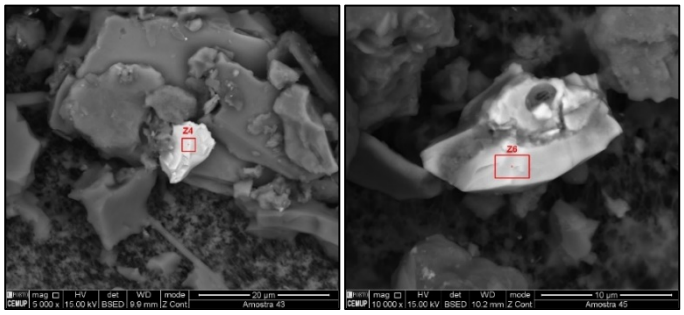

Figure 18. Scanning Electron Microscopy images of zircon particles.

Barium sulfate is a white crystalline solid, with the chemical formula $BaSO_4$. It is used in several industries: steel, chemical, paper, rubber, paint, plastics, glass, oil and natural gas industries. Barium sulphate particles were identified in SP1, SP2, SP3, SP5, SP7, SP10, SP11, SP14, SP21, SP23, SP26, SP29 and SP34 (Figure 19).

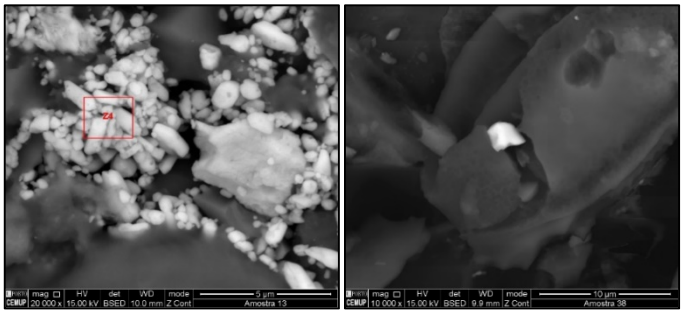

Figure 19. Scanning Electron Microscopy images of barium sulphate particles.

Strontium sulfate, $SrSO_4$, is of interest as a naturally occurring precursor to other strontium compounds, which are more useful. In industry, it is converted in carbonate (to be used as a ceramic precursor) and in nitrate (to be used in pyrotechnics). Strontium sulphate particles were identified only in SP9 (Figure 20).

Preprints (www.preprints.org) | NOT PEER-REVIEWED | Posted: 7 August 2020 doi:10.20944/preprints202008.0184.v1

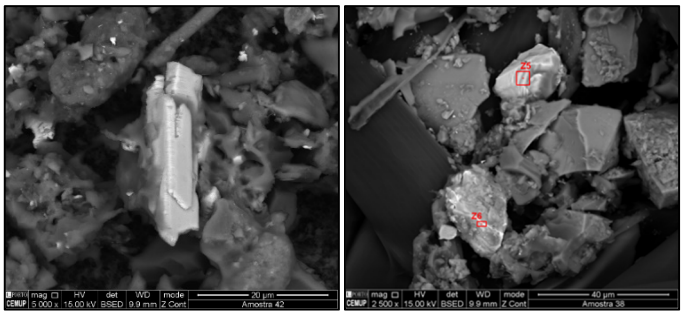

Figure 20. Scanning Electron Microscopy images of strontium sulphate particles.

Calcium carbonate ($CaCO_3$) is the most abundant non-silicate material in arid soils and is expected to be a major constituent in mineral dust aerosol. In the atmosphere, the particles of calcium carbonate will react with acid gasses to form calcium salts, such as the reaction with nitric acid to form hygroscopic $10Ca(NO_3)_2$. Calcium carbonate particles were identified in SP22 (Figure 21-a).

Apatite is a mineral in the phosphate group, with the following variants: hydroxyapatite, fluorapatite and chlorapatite. The generic chemical composition is $Ca_5(PO_4)_3(OH, F, Cl)$. It is used mainly for the production of chemical fertilizers and phosphoric acid. Apatite particles were identified in SP10 (Figure 21-b).

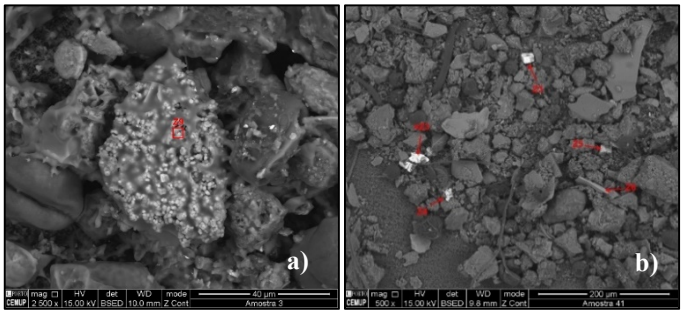

Figure 21. Scanning Electron Microscopy images of calcium carbonate particle-a) and apatite particles-b).

Monazite is a phosphate mineral that contains rare-earth elements (~70% REE). Due to variability in composition, (Ce, La, Nd, Th) (PO_4, SiO_4), monazite is considered a group of minerals. According to dominant REE contents, monazite is divided into monazite-(Ce), monazite-(La), monazite-(Nd), and monazite-(Sm), and the first type is most common in nature. It is a naturally occurring radioactive material (due to the presence of thorium and uranium). Monazite occurs as accessory minerals in igneous, metamorphic, and sedimentary rocks. Besides, monazite is found throughout the world in placer deposits, and beach sands. Monazite particles were identified in SP2, SP4, SP6, SP8, SP9, SP14, SP16, SP18, SP21, SP24, SP26, SP27, and SP33 (Figure 22).

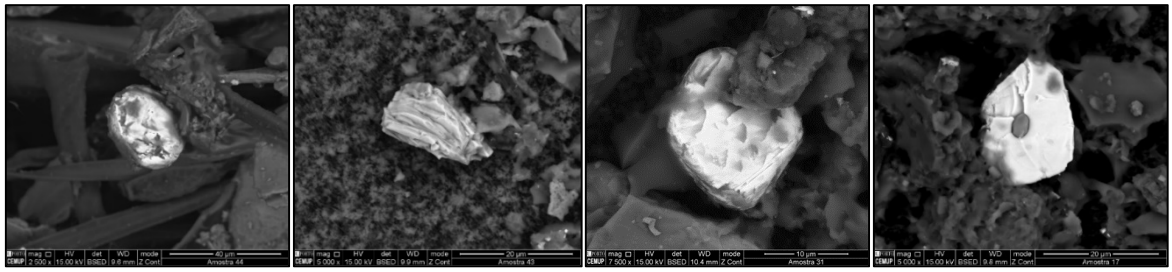

Figure 22. Scanning Electron Microscopy images of monazite particles.

Xenotime is a rare mineral composed of yttrium phosphate (YPO_4). Source rocks for xenotime are generally granites and pegmatites. When associated with classical monazite, tourmaline, rutile, and zircon, it reflects a predominantly granitic source. Xenotime is widely used in the manufacture of alloys, optical glass, and ceramics, in phosphors employed in television tubes and computer

Preprints (www.preprints.org) | NOT PEER-REVIEWED | Posted: 7 August 2020 doi:10.20944/preprints202008.0184.v1

monitors, in laser systems and as a catalyst for ethylene polymerization. Xenotime was found in SP1, SP8, SP11 and SP30 (Figure 23).

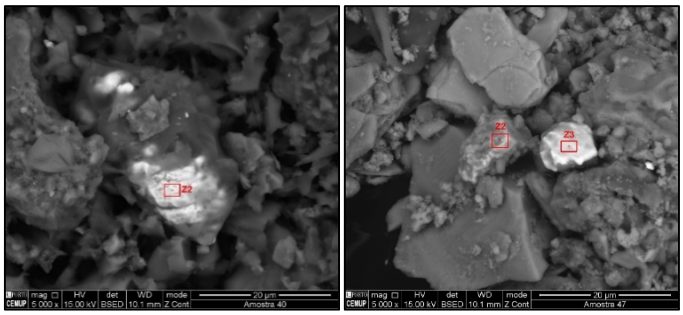

Figure 23. Scanning Electron Microscopy images of xenotime particles.

Copper is one of the essential metals at industrial level and is characterized by its red colour and particular properties such as electrical conductivity. Most of its uses are based on this property or the fact that it is also a good thermal conductor. However, many of its applications also rely on one or more of its other properties (e.g. corrosion-resistant, ductile, antibacterial, etc.). In urban environments, it is used mainly in electricity for cables and wires. It is also used in civil construction in roofs, gutters and window frames. Brake pads are responsible for a significant fraction of copper in urban dust as well. In this study, the subway which serves the campus is aboveground in several parts of the line. In other cases, the coal-fired furnaces used to heat private homes may also have contributed to the collected copper particles, identified in SP23, SP24, SP25 and SP27 (Figure 24-a and **Error! Reference source not found.**-b).

Pyrite (FeS_2) is an iron sulphide. In the past, pyrite was the main source of sulphur and sulphur dioxide used for bleaching, and in the production of sulphuric acid. Sulphuric acid applied to phosphate rock makes superphosphate for agriculture. In the clothing industries, pyrite produced the potassium aluminium sulphate alum indispensable in the chemical fixing of dyes to the cloth. Pyrite also provided an essential ingredient, sulphur, for gunpowder [8]. Pyrite particles were identified at SP7 (Figure 24-c).

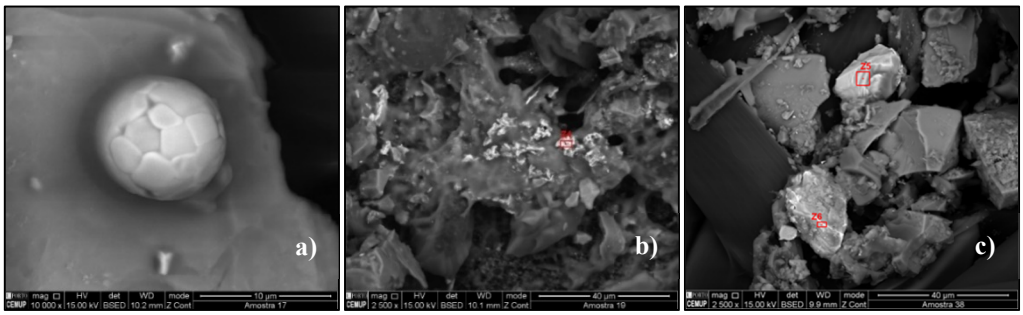

Figure 24. Scanning Electron Microscopy images of pure copper sphere 10 μm-a), copper particle 10 μm covered with resin-b) and pyrite-c).

Chromium is a naturally occurring element in rocks, animals, plants, soil, and volcanic dust and gases. Chromium occurs in the environment primarily in two valence states, trivalent chromium (Cr III) and hexavalent chromium (Cr VI). Exposure may occur from natural or industrial sources of chromium. Air emissions of chromium are predominantly of trivalent chromium and in the form of small particles or aerosols. The most important industrial sources of chromium in the atmosphere are those related to ferrochrome production. Ore refining, chemical and refractory processing, cement-producing plants, automobile brake lining and catalytic converters for automobiles, leather tanneries, and chrome pigments also contribute to the atmospheric burden of chromium [9]. Chromium particles were identified in SP28 (Figure 25-a).

Tin is a silvery, malleable metal, solid under environmental conditions, oxidizing easily with air and resistant to corrosion. As a pure metal, tin is used in the construction of tubes and valves, in the

Preprints (www.preprints.org) | NOT PEER-REVIEWED | Posted: 7 August 2020 doi:10.20944/preprints202008.0184.v1

manufacture of containers for distilled water, beer and carbonated drinks. It can also be used, for example, in storage tanks for pharmaceutical, chemical solutions, in condenser electrodes, fuses, ammunition, metallized paper to wrap food and tobacco. The tin powder is used in the manufacture of paints and sprays. Tin particles were identified at SP5 and SP24 (Figure 25-b and Figure 25-c).

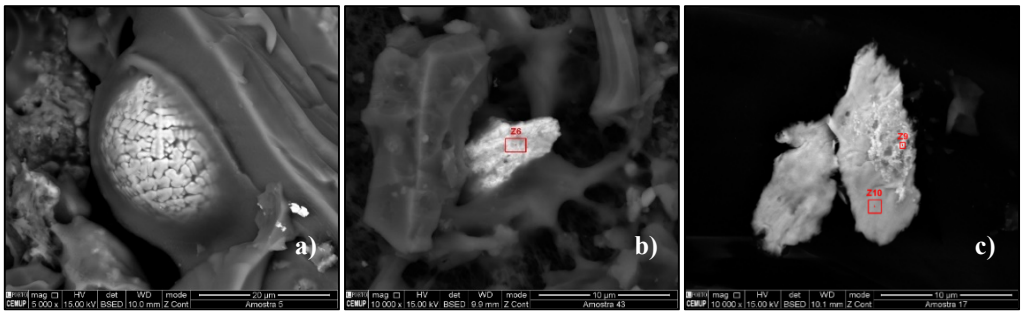

Figure 25. Scanning Electron Microscopy images of chromium particle-a) and tin particles-b) and c).

Iron (III) oxide or ferric oxide, also known as hematite (Fe_2O_3) it is important iron ore, with a metallic content of around 65%. Most of the iron oxides have their origin in the re-suspended road and soil dust. In urban environments, pulverized hematite is used for paint and polishing. Iron oxide particles were identified in the following sampling locations: SP3, SP4, SP5, SP6, SP7, SP8, SP9, SP10, SP11, SP12, SP13, SP14, SP15, SP16, SP17, SP18, SP19, SP20, SP21, SP22, SP23, SP24, SP25, SP26, SP27, SP28, SP29 (Figure 26).

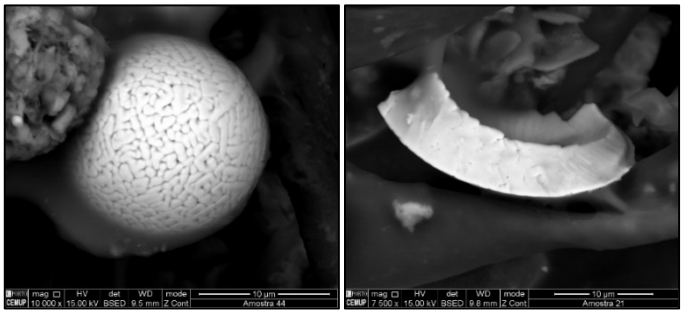

Figure 26. Scanning Electron Microscopy images of iron oxide particles.

Zinc oxide (ZnO) is an inorganic compound that appears as a white powder when pure, but in nature, it occurs as the rare mineral zincite, which usually contains manganese and other impurities that confer a yellow to red colour. It is used as an additive in numerous materials and products including cosmetics, food supplements, rubbers, plastics, ceramics, glass, cement, lubricants, paints, adhesives, sealants, pigments, foods, batteries, ferrites, fire retardants, and first-aid tapes. Although it occurs naturally as the mineral zincite, most zinc oxide is produced synthetically. Zinc oxide particles were identified at SP31 (Figure 27-a).

Pyrolusite (MnO_2) is the most commonly occurring manganese-bearing mineral (manganese dioxide), which is the most important manganese mineral (63% manganese). Manganese does not occur naturally as a base metal but is a component of more than 100 minerals. Crustal rock is a major source of manganese found in the atmosphere. The major anthropogenic sources of environmental manganese include municipal wastewater discharges, sewage sludge, mining and mineral processing (particularly nickel), emissions from alloy, steel, and iron production, combustion of fossil fuels, and, to a much lesser extent, emissions from the combustion of fuel additives. It is widely applied in the production of steel [10] and also used in electric batteries, glass, photographs and chemicals. Pyrolusite particles were identified at SP23 (Figure 27-b).

Preprints (www.preprints.org) | NOT PEER-REVIEWED | Posted: 7 August 2020 doi:10.20944/preprints202008.0184.v1

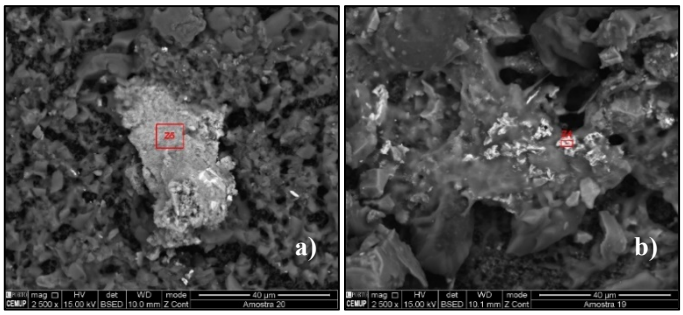

Figure 27. Scanning Electron Microscopy images of zinc oxide particle-a) and pyrolusite particle-b).

Titanium is a light metallic element white colour, glossy and resistant to corrosion. In most cases, it is used in the form of alloys with other metals such as aluminium, iron, manganese, chromium, molybdenum and vanadium. These applications represent 90% of the total production of titanium, and the remainder is for the construction of equipment (pumps, heat exchangers, etc.). The most important titanium compound, from an industrial point of view, is titanium dioxide which finds wide use as a pigment in the manufacture of paints, lacquers, enamels, paper, rubber, textiles, plastics, ceramics and cosmetics. Titanium particles were identified at SP1, SP5, SP7, SP17, SP21, SP25, SP26, SP27 and SP34 (Figure 28).

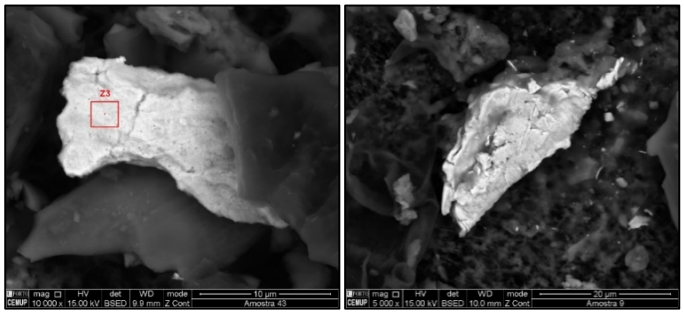

Figure 28. Scanning Electron Microscopy images of titanium particles.

Brass is a metallic alloy of copper and zinc. The general chemical formula of brass is Cu3Zn2. Other metals may be present, and according to their quantity and proportion, the properties of the alloy are different. Occasionally, small amounts of aluminium, tin, lead and arsenic can be added to enhance some of the properties of this alloy depending on its application. Brass is used in the manufacture of condenser tubes, weapons, ammunition cartridges, taps, radiator cores, medical and surgical devices, ornaments, jewellery, electrical terminals, coins, wires, valves, car wheels, and many others applications. It is also an important component of disk brake systems along with copper and steel. Brass particles were identified at SP1, SP5 and SP6 (Figure 29).

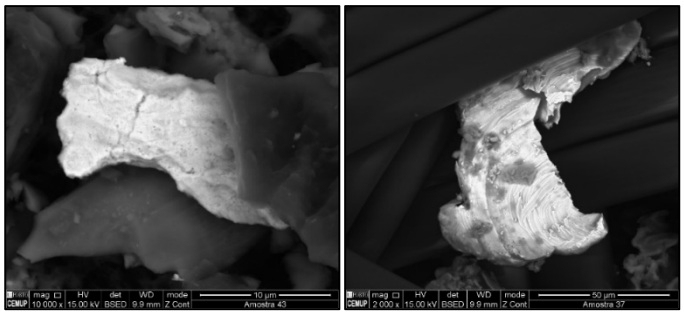

Figure 29. Scanning Electron Microscopy images of brass particles.

Stainless steel is a family of iron-based alloys with a minimum of 10.5% chromium, less than 1.2% carbon and other alloying elements. Chromium produces a thin layer of oxide on the steel surface, called a "passive layer" which prevents surface corrosion; the greater the amount of

Preprints (www.preprints.org) | NOT PEER-REVIEWED | Posted: 7 August 2020 doi:10.20944/preprints202008.0184.v1

chromium, the greater the corrosion resistance. Stainless steel can also contain others metals, such as nickel, molybdenum, titanium and copper, and non-metals, such as carbon and nitrogen, which can be added to improve other properties such as strengthening malleability and increasing corrosion resistance. Stainless steel can be used in the most different applications: home appliances (large appliances and small household items), automobiles (production of parts for vehicles), construction (buildings and furniture), in the food industry, in the chemical industry, oil industry and many others applications. Stainless steel particles were identified at all sampling points except SP8, SP12, SP15, SP16, SP17, SP22, SP25, SP27, SP28, SP30, SP32, SP33 (Figure 30).

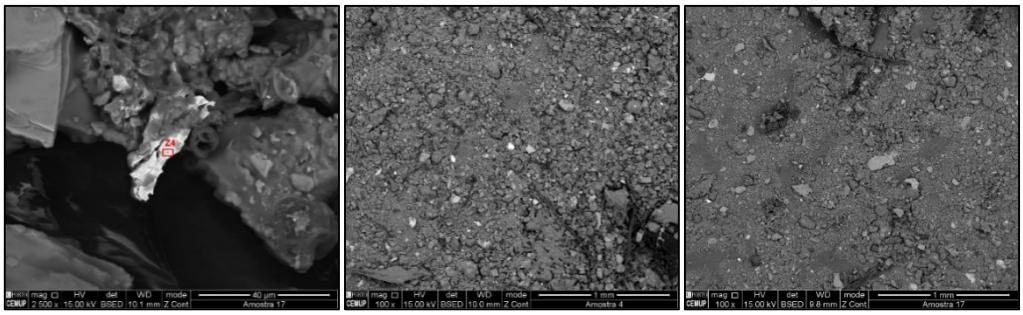

Figure 30. Scanning Electron Microscopy images of stainless steel.

In all sampling campaigns, there is recurrent higher deposition flux at some sampling locations: SP7, SP13, SP25 and SP28 (Table 9). Lower frequencies were observed in SP10, SP18, SP23, SP30, SP31 and SP33 followed by SP5, SP6, SP16, SP24, SP32 and SP34. In some cases, higher deposition fluxes were obtained in quite different seasons: SP10, SP13, SP28, SP30, SP31, SP33.

Table 9: Frequency of sampling points with higher deposition flux.

Sampling campaign Nº	**Sampling point Nº**															
2	--	--	7	10	13	--	--	--	24	--	28	30	31	32	33	--
3	5	6	7	--	13	16	--	23	--	--	28	--	--	--	--	--
4	--	--	7	--	--	--	18	--	--	25	--	--	--	--	--	--
5	--	--	7	--	--	--	18	--	--	25	--	--	--	--	--	--
6	--	--	--	--	--	--	--	23	--	--	--	--	--	--	--	--
7	--	--	7	10	13	--	--	--	--	25	28	30	31	--	33	34
Frequency	**1**	**1**	**5**	**2**	**3**	**1**	**2**	**2**	**1**	**3**	**3**	**2**	**2**	**1**	**2**	**1**

4. Discussion

Particulate matter deposition strongly depends on the climatological variables, and therefore it is expected that these variables have affected the deposition pattern during all sampling campaigns. In particular, the average temperature registered different values throughout the seven sampling periods. The temperature promotes the convective transport of the particles.

During the period under analysis, on most days, there was no record of precipitation, except in the 6th and 7th sampling campaigns, which can be considered as very rainy. The dry months favoured the suspension of particles in the atmosphere.

The wind speed was, on average, of low intensity and the direction was predominantly to the south which may explain the high deposition fluxes observed in some sampling points placed in this direction (SP30, SP31 and SP18).

Sampling campaigns Nº 2 and Nº 3 were carried out during a very hot and dry period, and presented the highest deposition fluxes: 2.04 g m^{-2} month^{-1} and 1.72 g m^{-2} month^{-1}, respectively. While lower deposition fluxes were registered for sampling campaign Nº 6 and Nº 7, characterized by continuous and intense rainfall events: 0.23 g m^{-2} month^{-1} and 0.24 g m^{-2} month^{-1}, respectively. Besides, during the sampling campaign Nº 6 the exposure period of the collectors was longer (~65 days) which lead to the washing of the particles and also to the loss of efficiency of the resin.

 doi:10.20944/preprints202008.0184.v1

In what concerns to the spatial variability of the deposition flux, it was observed a recurrent higher deposition flux at SP7 (FEUP-cafeteria), followed by SP13 (Crematorium), SP25 (grass field) and SP28 (Hospital S. João). These high flux values are mostly due to car parking and road traffic and the presence of chimneys. Lower frequency was observed in SP10 (FEUP-parking), SP18 (IPATIMUP-entrance), SP23 (ESE-parking), SP30 (ESEP-entry), SP31 (ESEP-parking) and SP33 (ISEP-buildings). These sampling points are also affected by road traffic, smoking spots and subway lines.

Regarding the results from the scanning electron microscopy, there are a few elements/compounds that were identified at the same sampling points for both sampling campaigns: stainless steel - SP27; monazite - SP4, SP14, SP24, SP27; barium sulfate - SP14 and iron (III) oxide - SP27. It appears that the existence of certain elements in different locations may be an indication of the same emitting source. It was not possible to extend the SEM analysis to all sampling campaigns but, although inconclusive, these results can be seen as indicators of the need to carry out a complete qualitative study of particulate matter deposition in the campus.

Copper and silicon found, for example, on the collector placed in the HSJ pediatric building, may have their origin in the construction works that were taking place at the site, since they are both used in civil construction, and in many cases, the construction activities and paved road dust have been identified as significant precursors of dust fallout in urban environments. Hence, it is important to analyze the material collected at same points but from different sampling campaigns, as these construction works did not take place during all the sampling campaigns, so the result of the analysis would be different if this were the origin. The copper found at SP24 may be originated from tobacco smoke, as this is a smoking area.

Titanium dioxide, zinc oxide, barium sulfate, tin, biotite and iron oxide are used as pigments in the manufacture of paints, and therefore their presence can be justified by the residues of paint from the places (electricity poles, columns, waterfall tubes) where the collectors were fixed.

Stainless steel and aluminosilicate were the compounds/elements most frequently identified in the scanning electron microscopy. As they have applications in the most diverse industries, it is expected to find their presence in almost all samples.

Monazite, a mineral that corresponds to phosphate and which is a source of metals and rare earths, was found in samples located in HSJ, FEUP, FADEUP and ESE, very close to each other. This mineral can have a natural origin because it is part of the accessory minerals of the granite of Porto (for example, degradation of monuments). Besides being common in some sands (monazite sands), these type of sands does not occur in Portugal. This mineral may also have an anthropogenic origin, for example in the wear of road pavement. The sources of anthropogenic particles with monazite can be broken down based on their morphological and mineralogical characteristics and also grain size.

Calcium carbonate was observed in SP22 (ESE), and as previously mentioned, it is the main constituent of mortar, widely used in civil construction. This sampling point is very close to SP27, where construction works were taking place, and therefore there may be a connection between both.

Brass was found at FEUP: SP1, SP5 and SP6, locations characterized by the proximity to several car park and roads. Brass has several applications and, in this case, its source may from the structure of the vehicle passing by.

Finally, it is possible to verify the presence of titanium, and silicon particles in SP17 (FADEUP soccer field), SP25 (ESE) and SP27 (HSJ Pediatric building), which are elements used in the ceramic industry, and possibly have the same emitting source. The same can be seen at SP23 (ESE car park), where pyrolusite, barium sulfate and aluminosilicates were identified.

5. Conclusions

A simple passive particle collector of urban dust for estimating the deposition flux was used. It was possible to identify the most problematic locations at the campus for air quality, in what concerns the amount of particulate matter deposition. Some mitigation measures may be suggested to redirect the concentration of people at some spots, like the smoking ones. In what concerns to the road traffic, the desire would be a reduction and a limitation of vehicle access in all campus.

The identification of emitting sources of particulate deposition in urban environments is one of the significant challenges posed by air quality assessment. In this study, the results raised many questions that must be further investigated in future work which be much more complete with a chemical analysis of all samples and particle size determination in all sampling points (PM2.5 and PM10).

Conflicts of Interest: The authors declare no conflict of interest.

References

1. U.S. EPA. Air Quality Criteria for Particulate Matter (Final Report, 1996). U.S. Environmental Protection Agency, Washington, D.C., EPA 600/P-95/001.
2. Xing, Y.F.; Xu, YH; Shi, MH; Lian, Y.X. The impact of PM2.5 on the human respiratory system. J Thorac Dis. 2016 Jan; 8(1): E69-E74. DOI: 10.3978/j.issn.2072-1439.2016.01.19.
3. World Health Organization Regional Office for Europe. Air Quality Guidelines, 2nd ed.; WHO regional publications; Copenhagen, Denmark, 2000; No. 91, Chapter 7.3, pp. 186-193.
4. Colls, J.; Tiwary, A. Air pollutants: Pollution - Measurement, modelling and mitigation, 3rd ed.;. Oxon. Routledge. 2010; pp. 54-88.
5. Van Malderen, H.; Van Grieken, R.; Bufetov, N.V.; Koutzenogii, K.P. Chemical Characterization of Individual Aerosol Particles in Central Siberia. Environ. Sci. Technol. 1996; 30: 312-321.
6. Cong, Z.Y.; Kang, S.C.; Dong, S.P.; Liu, X.D.; Qin, D.H. Elemental and individual particle analysis of atmospheric aerosols from high Himalayas. Environ. Monit. Assess. 2010; 160, 323. DOI: 10.1007/s10661-008-0698-3.
7. Walkden, S.; Kelley, R.; Parrish, M.; Horstwood, A.; Indares, J.; Still, J. Determining Source of Ejecta Using Heavy Mineral Provenance Techniques; A Manicouagan Distal Ejecta Case Study. Earth Planet Sc Lett 2009; 285(1-2), pp. 163-172.
8. Don Emerson (2019) Pyrite - the firestone, Preview 2019; 203, 52-64. doi:10.1080/14432471.2019.1696247.
9. Zereini, F; Wiseman, L.S. Urban Airborne Particulate Matter, Origin, Chemistry, Fate and Health Impacts, 1st edition; Springer-Verlag Berlin Heidelberg, Germany, 2010.
10. World Health Organization Regional Office for Europe. Manganese and its Compounds: Environmental Aspects; Concise International Chemical Assessment Document 63; Geneve, 2004.